SolarPACES 2023, 29th International Conference on Concentrating Solar Power, Thermal, and Chemical Energy Systems

Power Cycles

https://doi.org/10.52825/solarpaces.v2i.841

Published: 18 Oct. 2024

Variation of Heliostat Wind Loads in a Radial Field Array Model

Matthew Marano[1], Matthew Emes[1], Azadeh Jafari[1], and Maziar Arjomandi[1]

[1] School of Electrical and Mechanical Engineering, University of Adelaide, Australia.

*Correspondence: Matthew Marano, matthew.marano@adelaide.edu.au

Abstract. The design of heliostats throughout a concentrated solar power (CSP) plant are currently of uniform design, however, research into the variation in heliostat wind loading within a radially staggered field array can provide insight into potential material cost savings in heliostat field design. Experimental investigation was carried out on a field array model in the University of Adelaide large wind tunnel. A total of 64 heliostat models of size 0.1 × 0.1 m were radially arranged over four surround rows. Four 3-axis load cells were utilized to analyze field array cases of morning (0700 hours), noon (1200 hours), and evening (1700 hours) configurations. Angle calculations for beam reflection were made for the 21st March (equinox). Results show mean and peak drag force coefficients reduce with distance into the field for a 1700 hour case due to high upstream blockage. Comparing the downstream drag and lift force coefficients against each test configuration, when heliostats are at steep elevation angles, high flow blockage leads to a reduction of coefficients downstream (0700 hour and 1700 hour cases). When elevation angles are reduced (1200 hours), drag and lift coefficients increase with distance from the central tower in the downstream direction. Results also show the central tower increases load coefficients on downstream heliostats, and therefore should be considered in heliostat wind loading and field design.

Keywords: Heliostat Wind Loads, Lift Force, Drag Force, Coefficients, Heliostat Array, Load Variation, Receiver Design

1. Introduction

Heliostats throughout a Concentrated Solar Power (CSP) plant are currently arranged to optimize optical performance [1]. The arrangement of heliostats based on wind loading is not considered. Currently, heliostats throughout a field are of uniform design based on single heliostat wind loads. As the cost of heliostat structure accounts for 34 - 50% of the setup cost of a CSP plant [2], [3], reducing the cost of the heliostat structure will lead to significant savings. The heliostat structure is designed to withstand wind loading and reduce vibrations, of which can lead to structural failure and beam misalignment [4]. Heliostat design can be optimized by considering a heliostat's position within a CSP field array. Wind load measurements in field show a 20 - 25% reduction in wind loading, in comparison to first row measurements [5]. Cermak et al. [6], and Ewald et al. [7] investigated heliostat array configurations. The main focus in literature has been to reduce heliostat wind loads using additional heliostat attachments, or fences in field to break up turbulence. Even though evidence exists that heliostats located in a field array have a reduced wind loading compared to individual and first row heliostats, previous wind tunnel experiments have primarily considered linearly configured arrays. This research aims to experimentally investigate the wind load variation on heliostats upstream and downstream of a tower in a radially staggered field array.

2. Methodology

A radial heliostat field model was designed and manufactured for experimentation in the University of Adelaide large wind tunnel. Maximizing the available space in the wind tunnel (3 × 3 m), the model base has a diameter of 2.7 m. Four three-axis load cells were utilized to analyze the variation in wind loading throughout the field. The load cells have a measurement rating of ± 2 N (K3D40 three-axis) and an accuracy of 0.2 %. Two ME-Systeme (GSV-1A8) DAQs sample the four load cells simultaneously at a frequency of 1 kHz. Inflow characteristics were measured using a Turbulent Flow Instrumentation (TFI) multi-hole pressure (Cobra) probe with a sampling rate of 2 kHz, and an accuracy of ± 0.3 m/s. The flow speed and load cell specifications limit the size of the heliostat on the model. Therefore, for a maximum flow speed of 12 m/s, a heliostat size of 0.1 × 0.1 (0.01 m^2) was determined. To model a radially staggered heliostat field for heliostats of this size, row radii are set at 0.5 m, 0.71 m, 0.95 m, and 1.22 m, with a central tower height of 1 m (diameter of 50 mm) for a no blocking configuration (Figure 1a) [8]. Each heliostat is radially spaced by 22.5 degrees, as seen in Figure 1a. A total of 64 heliostats can be radially staggered around the central tower. To gain an understanding of the variation in wind loading throughout the field, the instrumented section with four load cells can be repositioned to one of the 16 sections around the model, for a given configuration. The load cells are secured on a secondary platform, beneath the top surface, isolated form the incoming flow, as seen in Figure 1b, with the load cell fixed atop of a rigid steel plate. The pylon is made from aluminum to keep the model light weight to maximize the available capacity of the sensors. To keep the hinge cross section to a minimum, the heliostat panel and hinge are 3D printed. The design of the pylon and heliostat panel allows for 3 degrees-of-freedom, giving the option of variable hinge height, azimuthal angle, and elevation angle.

(a) (b)

Figure 1. *(a) Top-down view of the heliostat field array model with the heliostats in a stowed position. The row radii and azimuthal spacing are highlighted on the image. The blue taped region indicates the position of the load cells for the test configuration. (b) Close up of an instrumented heliostat mounted beneath the model top surface. The cover plate to shelter the load cell is displayed to the left.*

The heliostats were oriented for a field located at the equator on the 21st March (equinox), meaning the sun passes directly over the centerline of the field. The test cases of morning (0700 hours), noon (1200 hours), and evening (1700 hours), were configured for experimentation. The resulting elevation angles for the instrumented heliostats is shown in Figure 2. The azimuthal angles were transformed to an angle in relation to the tower for consistent setting of the heliostat azimuthal angles using a protractor. The resultant azimuthal angles (β) have a variation of $\pm 11°$ across the instrumented heliostats for each configuration. The elevation angle was set in relation to the model base using 3D printed wedges. Therefore, an accuracy of ±1° was achieved for both angles. The implemented heliostat arrangement for experimentation was as shown in Figure 3.

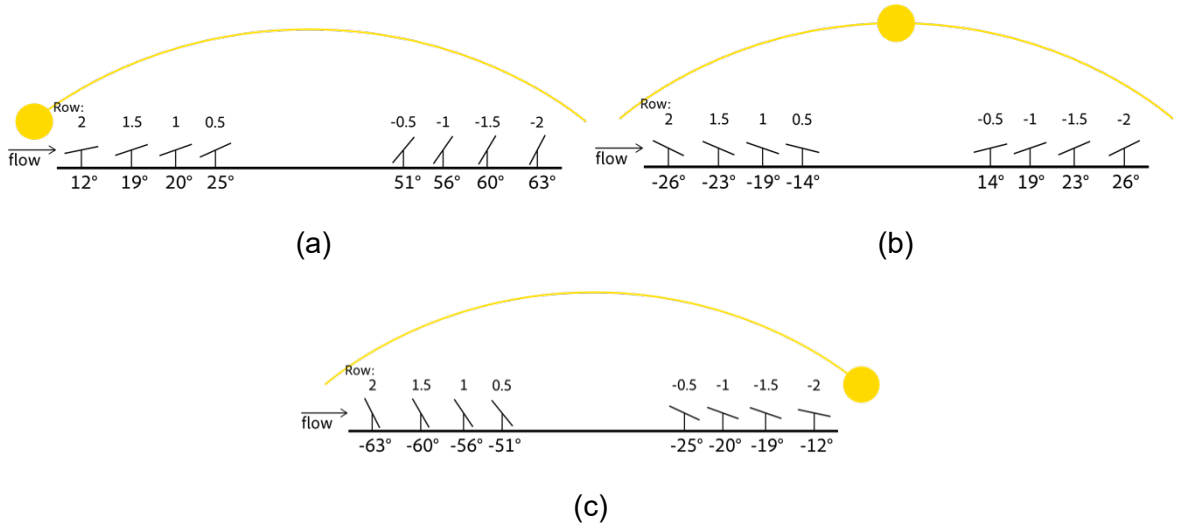

Figure 2. *Instrumented heliostat elevation (α) angles for; (a) morning (0700 hours), (b) noon (1200 hours), and (c) evening (1700 hours) test cases. The row numbers are indicated for reference with positive being upstream, and negative being downstream, from the central tower.*

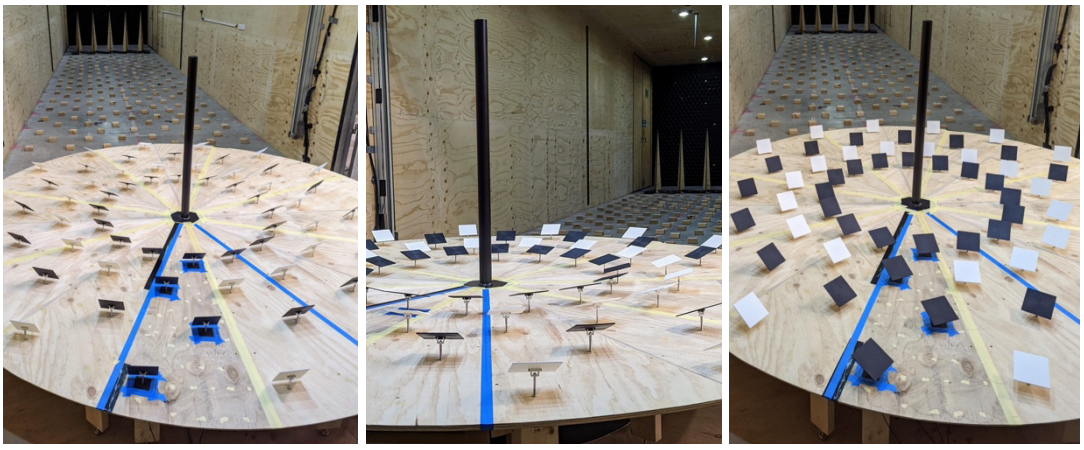

Figure 3. *Images of the model heliostat field setup in the University of Adelaide wind tunnel for (a) morning, (b) noon, and (c) evening cases. The instrumented heliostats are highlighted with blue tape.*

Three experimental load recordings were captured over 2-minute periods. Wind loads were measured about three orthogonal axes F_x, F_y, and $\mathrm{F_z}$ (Figure 4). Coefficients derived from the measured forces were nondimensionalized using Equation 1.

$$C_{F_{x,y,z}} = F_{x,y,z} / \left(\frac{1}{2}\rho U^2 A\right) \quad (1)$$

Where $F_{x,y,z}$ are the forces measured by the load cell in the respective axis in Figure 4, ρ is the air density equal to 1.25 kg/m^3, U is the velocity equal to 9.6 m/s at the heliostat hinge height of 0.05 m, and A is the total heliostat mirror area (0.1 m × 0.1 m). Peak coefficients are calculated as the sum of the mean and three times the standard deviation, giving a 99.7% confidence value of not being exceeded [9].

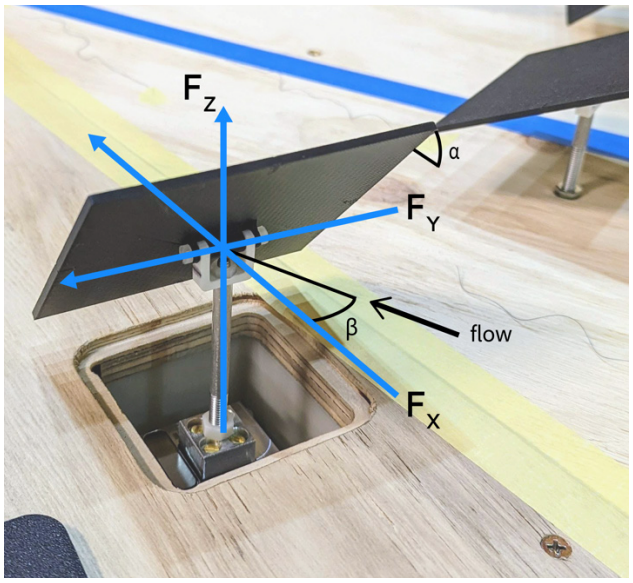

Figure 4. *Schematic diagram of all relevant forces acting on the heliostat due to exposure to wind.*

3. Results

Results show the drag (x-axis) and lift (z-axis) force coefficients, for a hinge height velocity of 9.6 m/s. Wind loading within a radially staggered field array varies depending on array configuration (time of day) and flow direction over the field. All results are for the specified time of day with the wind approaching from the east, for a field located at the equator. Due to the heliostat array configuration, 0700 hours is identical to 1700 hours only flipped about the central spanwise axis of the field. For example, the heliostat field array configuration for flow approaching to the east at 0700 hours is identical to the 1700 hours case with flow approaching from the west. This effectively doubles the experimented cases. For a noon configuration, as all elevation angles are identical per row, and all heliostats are directed towards the tower, the coefficients would apply to flow approaching from almost any direction due to a symmetry of the field every 22.5°.

Mean drag force coefficients decrease with distance over the field, as seen in Figure 5. The 1700 hour configuration has relatively steep heliostat elevation angles upstream (α = 63° to 51° from row 2 to 0.5) compared to other configurations, resulting in high upstream blockage. This high blockage reduces the mean windspeed in the field [5]. As the heliostat elevation angles are also decreasing over the length of the field, the frontal area of a heliostat is reduced leading to a further reduction in drag force coefficient, compared to upstream heliostats. Peak drag coefficients follow a similar trend as the mean values, however, this trend has a maximum coefficient in the second row (row number 1.5). There is an average increase in standard deviation of fluctuating load of 97% from row 2 to row 1.5. This can be linked to an increase in turbulence intensity resulting from vortex shedding of the upstream heliostat [5].

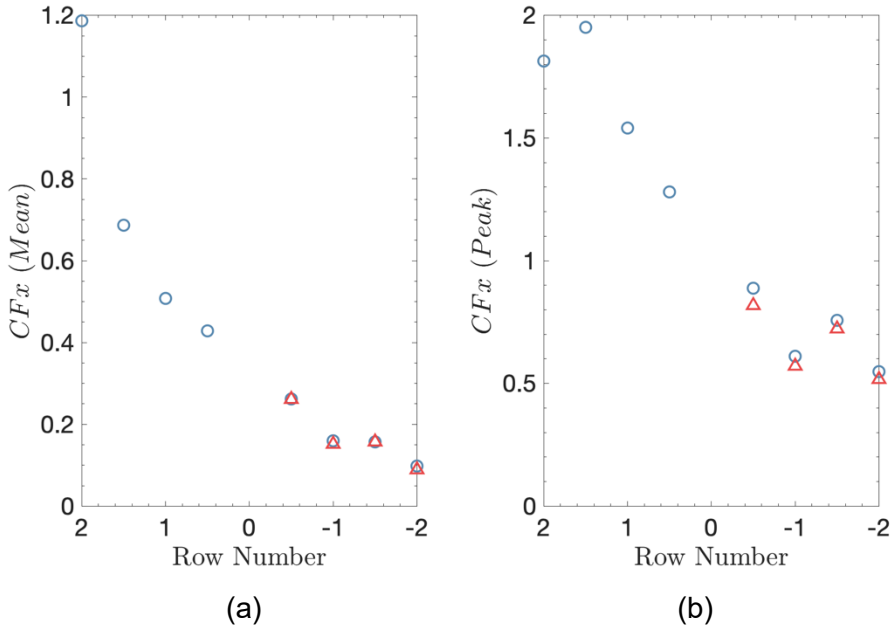

Figure 5. *Absolute (a) mean, and (b) peak absolute coefficients of drag force for a 1700 hour configuration, where circles indicate the central tower is installed, and triangles indicate the central tower is removed.*

Analyzing the change in lift force coefficient identifies a different trend to the drag force coefficient. Figure 6a shows a large relative decrease in lift between first (row number 2 and -0.5) and second rows (row number 1.5 and -1) of the upstream and downstream sections respectively. The coefficient of lift decreases from the first row, then remains relatively constant across the upstream section, with a slight increase for the innermost row upstream (row 0.5). As seen in Figure 2c the elevation angles of the downstream heliostats correspond to the cases where maximum lift occurs, this being a cause for the increase in coefficients compared to the upstream section [10], [11]. The distance between consecutive heliostat rows impacts the flow recovery, leading to increased unsteady component of loads compared to the first row [12]. Due to the effects of upstream, and spanwise heliostats, the flow characteristics at row -0.5 are not expected to recover to that upstream at row number 2.

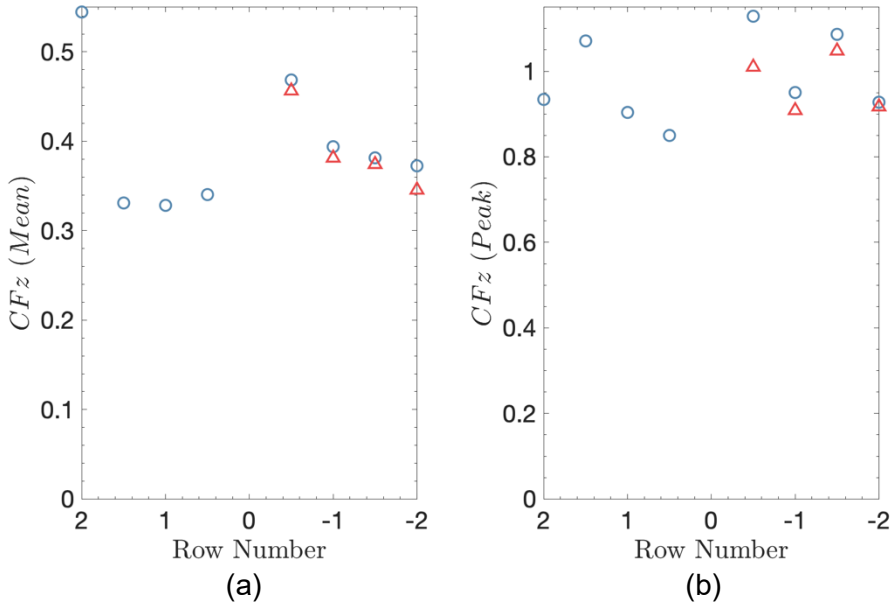

Figure 6. *Absolute (a) mean, and (b) peak coefficients of lift force for a 1700 hour configuration, where circles indicate the central tower is installed, and triangles indicate the central tower is removed.*

Figure 5 and Figure 6 show the effects of the central tower on the coefficients. On average, the mean and peak force coefficients decrease with the removal of the central tower by 5% when the tower is removed. The effects of the tower are more significant for peak lift coefficients. This indicates the central tower is shedding vortices, increasing the turbulence intensity and therefore fluctuation in wind loading. This indicates that the design of the central tower has an effect on heliostat wind loading. This is something that can be considered in layout and design of heliostats in the inner field region of a CSP plant.

Comparing the coefficients in the downstream section in Figure 7 and Figure 8, with a central tower installed for different times of day, identifies that wind loading does not exclusively decrease with an increase in the number of heliostats upstream. The magnitude of both drag and lift force coefficients, respectively, decrease for morning (0700) and evening (1700) array configurations downstream of the tower. This is due to the high elevation angles leading to high flow blockage. Morning drag force coefficients have higher magnitudes in comparison to the evening due to the low upstream blockage at 0700 hours. The coefficient of lift force is greater at 1700 hours compared to 0700 hours in the downstream section due to heliostat elevation angles being closer to the angle of maximum lift ($\alpha = 30°$) [10], [11].

The noon case (1200 hours) shows that both drag and lift force coefficients increase downstream. This indicates how wind loading can vary throughout a field array. For the noon configuration (Figure 2b), elevation angles have smaller variation between rows and are generally lower in magnitude compared to the 0700 and 1700 hour configurations. This results in less flow blockage upstream, causing higher mean flow speed and greater wind loading compared to the other cases. Therefore, as the elevation angles increase from 14° to 26° in the rows downstream of the tower, the load force coefficient magnitudes increase with distance from the tower. Peak coefficients are sufficiently large (Figure 8) regardless of elevation angle. This is linked to the increase of turbulence intensity in the field [5], increasing the peak coefficients with the estimation method used [9]. Flow measurements between rows would confirm the increase in turbulence intensity.

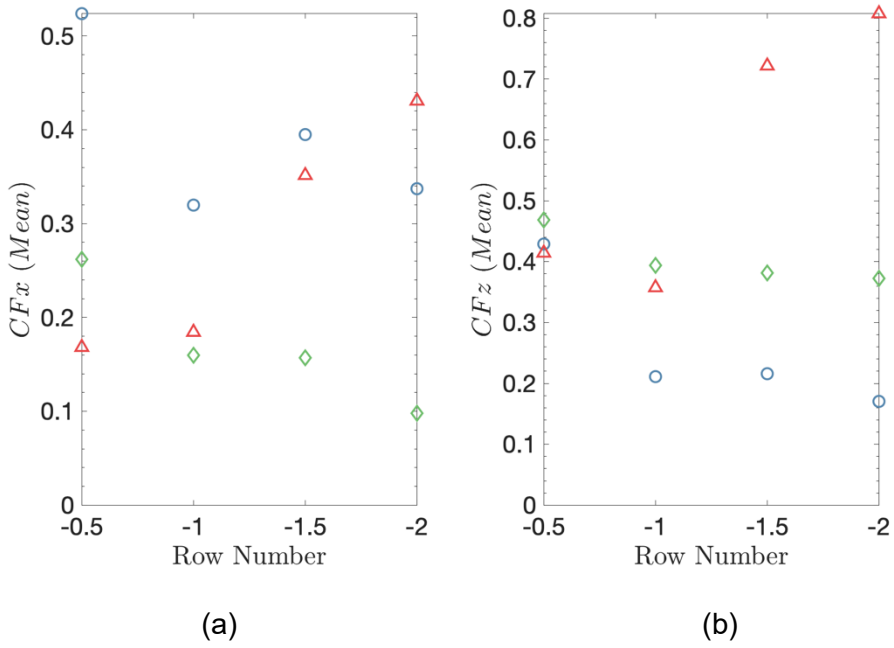

Figure 7. *Comparison of mean coefficients (absolute) of (a) drag force, and (b) lift force, for all configurations, where circles represent a 0700 hour case, triangles a 1200 hour case, and diamonds represent a 1700 hour case.*

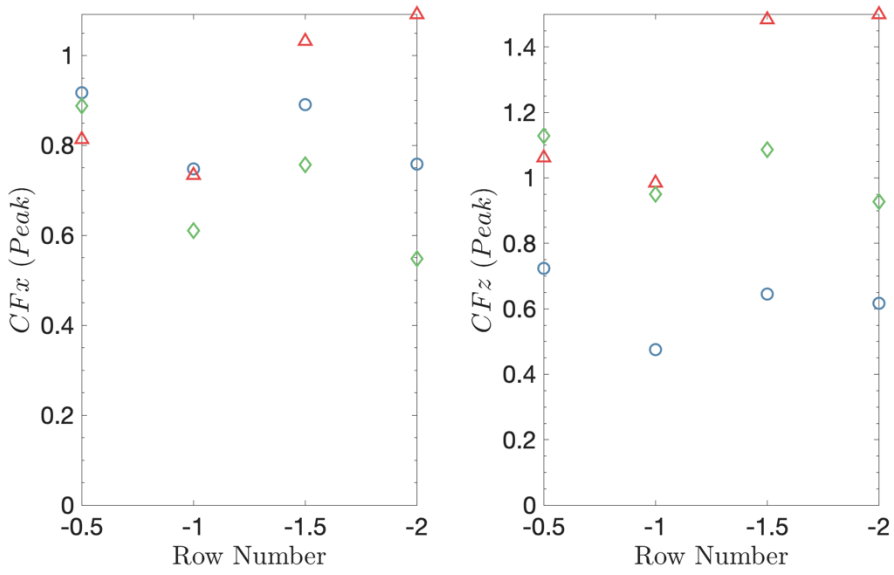

Figure 8. *Comparison of peak coefficients (absolute) of (a) drag force, and (b) lift force, for all configurations, where circles represent a 0700 hour case, triangles a 1200 hour case, and diamonds represent a 1700 hour case.*

4. Conclusion

Wind load coefficients derived in wind tunnel experiments through drag and lift forces measured on four heliostats in different rows within a radial heliostat field array vary depending on the time of day. For an easterly wind direction, mean drag and lift force coefficients on heliostats in a downstream region of the field decrease for early morning and evening cases, compared to the first row coefficients. Midday configurations will be similar regardless of the flow direction, due to all elevation angles being consistent for each row. These results suggest that in-field heliostats can be designed for a reduced wind load compared to those in the outer rows. If wind characteristics for a CSP plant site has a prevailing wind direction, the heliostats in the inner field region may not be required to be designed to withstand wind loads as that of a single heliostat. The central tower has an effect on downstream heliostat wind loading. The tower profile should be considered in heliostat field design, as it is evident that peak drag and lift force coefficients increase downstream due to the presence of the tower.

Data availability statement

Data in the article can be accessed by contacting the authors.

Author contributions

Matthew Marano contributed to conceptualization, data curation, formal analysis, investigation, methodology, software, visualization, and writing (original draft). Matthew Emes contributed to conceptualization, investigation, methodology, supervision, validation, and writing (review). Azadeh Jafari contributed to conceptualization, investigation, supervision, and validation. Maziar Arjomandi contributed to conceptualization, investigation, supervision, and validation.

Competing interests

The authors declare that they have no competing interests.

Funding

Funding was provided by the Australian Renewable Energy Agency (ARENA) [grant number 1-SRI002].

Acknowledgement

The authors acknowledge the support received for this research through the provision of an Australian Government Research Training Program Scholarship. The authors would also like to acknowledge the support received from the Australian Solar Thermal Research Institute (ASTRI) and funding provided by the Australian Renewable Energy Agency (ARENA) [grant number 1-SRI002].

References

1. M. Emes, A. Jafari, A. Pfahl, J. Coventry, & M. Arjomandi (2021). A review of static and dynamic heliostat wind loads, Solar Energy, vol.225.
2. P. Kurup, S. Akar, S. Glynn, C. Augustine & P. Davenport (2022). Cost Update: Commercial and Advanced Heliostat Collectors, National Renewable Energy Laboratory, Report: NREL/TP-7A40-80482.
3. A. Pfahl, J. Coventry, M. Röger, F. Wolfertstetter, J.F. Vásquez-Arango, F. Gross, M. Arjomandi, P. Schwarzbözl, M. Geiger & P. Liedke (2017). Progress in heliostat development, Solar Energy, vol.152, doi:10.1016/j.solener.2017.03.029.
4. M. J. Emes, A. Jafari, J. Coventry & M. Arjomandi (2020). The influence of atmospheric boundary layer turbulence on the design wind loads and cost of heliostats", Solar Energy, vol.207, pp.796-812, Sept, 2020, doi:10.1016/j.solener.2020.07.022.
5. J. Peterka, N. Hosoya, B. Bienkiewicz, & J. Cermak (1986). Wind load reduction for heliostats: a subcontract report, Colorado State University, United States.
6. J. Cermak, J. Peterka & A. Kareem (1978). Heliostat field array wind tunnel test, Colorado State University, United States.
7. R. Ewald, J. Peterka & J. Cermak (1979). Heliostat-array wind-tunnel study, Colorado State University, United States.
8. F.J. Collado & J.A. Turegano (1989). Calculation of the annual thermal energy supplied by a defined heliostat field, Solar Energy, vol.42, pp. 149-165, doi:10.1016/0038-092X(89)90142-4.
9. E. Simiu & R.H. Scanlan, (1996). Wind effects on structures: fundamentals and applications to design, John Wiley New York, Vol. 688.
10. M.J. Emes, A. Jafari, F. Ghanadi & M. Arjomandi (2019). Hinge and overturning moments due to unsteady heliostat pressure distributions in a turbulent atmospheric boundary layer, Solar Energy, vol.193, doi:10.1016/j.solener.2019.09.097.
11. J. Peterka, Z. Tan, J. Cermak & B. Bienkiewicz (1989). Mean and peak wind loads on heliostats, Journal of Solar Energy Engineering, vol.111, doi:10.1115/1.3268302.
12. A. Jafari, M. Emes, B. Cazzolato, F. Ghanadi & M. Arjomandi (2020). Turbulence characteristics in the wake of a heliostat in an atmospheric boundary layer flow, Physics of Fluids, vol.32.